TABLE II

FRACTION OF Co(III) IN THE FORM OF *cis*- AND *trans*-$Co(NH_3)_4H_2OCl^{2+}$ AS A FUNCTION OF TIME AT 15.8° AND 1 *N* $HClO_4$

Time,[a] sec	Fraction of *cis*	Fraction of *trans*, β
201	0.06	0.02
218	0.06	0.03
405	0.10	0.06
440	0.12	0.06
595	0.14	0.19
848	0.22	0.09
865	0.17	0.14
990	0.23	0.12
1443	0.35	0.13
1752	0.34	0.20
1792	0.34	0.20
1970	0.40	0.18
2485	0.52	0.15
2793	0.52	0.18
2918	0.55	0.17
3402	0.55	0.22
3910	0.68	0.14
3986	0.71	0.12
4831	0.69	0.19
5705	0.84	0.07

[a] The time elapsed between the initiation of the aquation and the quenching of it by Fe(II).

form. Since the rate constant for the aquation of *trans*-$Co(NH_3)_4Cl_2^+$ is known,[17] the fraction of the total Co(III) in this form can be calculated; by difference, then, the fraction of Co(III) in the form of *trans*-$Co(NH_3)_4H_2OCl^{2+}$ can be obtained. The results of these experiments are listed in Table II.

Stereochemistry of the Aquation of *trans*-$Co(NH_3)_4Cl_2^+$.—If it is assumed that the aquation of *trans*-$Co(NH_3)_4Cl_2^+$ can be represented by the equations

$$trans\text{-}Co(NH_3)_4Cl_2^+ \xrightarrow{k_1} x(trans\text{-}Co(NH_3)_4H_2OCl^{2+}) + (1-x)(cis\text{-}Co(NH_3)_4H_2OCl^{2+}) \quad (1)$$

$$trans\text{-}Co(NH_3)_4H_2OCl^{2+} \underset{k_3}{\overset{k_2}{\rightleftharpoons}} cis\text{-}Co(NH_3)_4H_2OCl^{2+} \quad (2)$$

then the pertinent differential equations can be integrated to yield

$$\beta = \left[\frac{k_1x - k_3}{k_2 + k_3 - k_1}\right]e^{-k_1t} + \left[\frac{k_3}{k_2 + k_3}\right] - \left[\frac{k_1(k_2x + k_3x - k_3)}{(k_2 + k_3)(k_2 + k_3 - k_1)}\right]e^{-(k_2+k_3)t} \quad (3)$$

where β is the fraction of the total Co(III) in the form of *trans*-$Co(NH_3)_4H_2OCl^{2+}$. Of the terms in eq 3, all can be obtained from the data reported above except x: k_1 is found in Table I; k_3 is obtainable from the Fe(II)-independent term in the reduction of *cis*-$Co(NH_3)_4H_2OCl^{2+}$;[12] k_2 results from the equilibrium constant of reaction 2, 9.6, and the value of k_3; and β as a function of time is given in Table II. Therefore, a plot of β *vs.* time for various values of x can be compared with the experimental data listed in Table II. Figure 1 contains a plot of the data and the theoretical curves for two values of x. Although the precision of the data is not good, it is clear that a value of x other than unity is required to fit the experimental points. The best value for x appears to be 0.45 ± 0.10 at 15.8° in 1 *N* $HClO_4$. This result disagrees with the original report of Tsuchida,[10] although it is not apparent that his data are incompatible with the result.

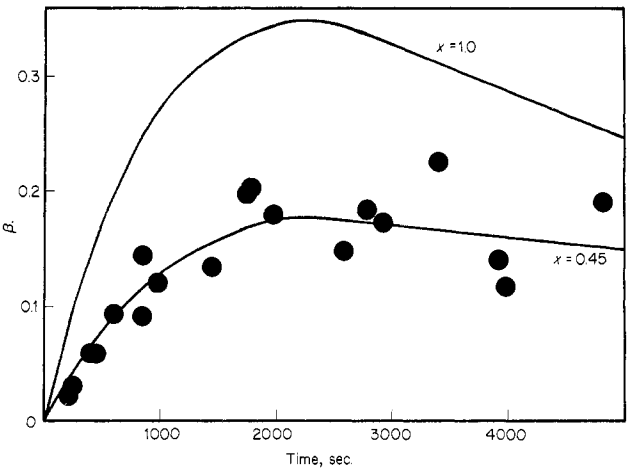

Figure 1.—The fraction of Co(III) in the form of *trans*-$Co(NH_3)_4H_2OCl^{2+}$, β, as a function of time, compared with theoretical curves for $x = 1.0$ and $x = 0.45$.

What the stereochemical consequences of the aquation of *trans*-$Co(NH_3)_4Cl_2^+$ demonstrate is that the ethylenediamine rings in the corresponding chelated cobalt(III) tetraammines[11] do not have a dominating effect upon the stereochemistry of aquation reactions. Further, the activation parameters for the aquation of *trans*-$Co(NH_3)_4Cl_2^+$ fit Tobe's correlation:[2] positive values of the entropy of activation are associated with a change in stereochemical configuration. What is still puzzling is why the free energy of activation varies as it does with a change in the coordination sphere of the Co(III) center.

Acknowledgment.—This work was supported in part by a grant from the National Institutes of Health (GM-14830).

(17) The concentration of Fe(II) added was sufficient to react with the *trans*-$Co(NH_3)_4Cl_2^+$ present rapidly enough so as to ensure negligible aquation during the reduction.

CONTRIBUTION FROM THE NATIONAL INSTITUTE OF ARTHRITIS AND METABOLIC DISEASES, NATIONAL INSTITUTES OF HEALTH, BETHESDA, MARYLAND 20014

Low-Temperature Raman Spectra of Solid Osmium Tetroxide and Ruthenium Tetroxide

BY IRA W. LEVIN

Received October 17, 1968

Several recent discussions of the Raman spectra of osmium tetroxide and ruthenium tetroxide report similar multiplet features for both species in the solid

phase.[1,2] The splitting pattern for OsO_4,[1,2] however, exhibits fewer lines than the number predicted from crystal field effects. In this communication we examine the solid Raman spectra, at liquid nitrogen temperatures, of both OsO_4 and RuO_4 and interpret the crystal fine structure as the complete removal of the normal mode degeneracies of the free molecule through static field and factor group, or correlation field, splittings.

Raman spectra were recorded with a Cary Model 81 spectrophotometer equipped with a helium–neon laser for irradiating the sample. Films of either OsO_4 or RuO_4 were sublimed onto a copper plate in contact with a liquid nitrogen reservoir. The deposition plate, enclosed within an evacuated glass cell, was fixed at approximately 45° to the front window of the cell, a glass optical flat. The entire cylindrical glass surface about the deposition plate, containing a sample inlet tube, rotates on a ground-glass joint in order to remove the inlet capillary from the optical path.[3] The laser beam then passes directly through the curved glass surface of the cell and focuses on the sample plate; the Raman emission is collected through the optical flat at 90° to the incident beam. Deposition times for the films ranged from several minutes to 0.5 hr. The films were routinely annealed several times. The reported vibrational frequencies are accurate to ± 2 cm^{-1}.

Since OsO_4 belongs to the space group C^6_{2h} with four molecules in the unit cell,[4] the Raman- and infrared-active vibrations of the crystal are determined by correlating the symmetry species of the isolated tetrahedral system and the C_{2h} factor group with the species of the C_2 site group. Table I displays the correlation diagram for OsO_4 with the result that in the site approximation the static crystal field lifts the degeneracies of the free molecule. Further, as a consequence of molecular interactions, each site component splits into two modes, namely, the symmetric (Raman-active) and antisymmetric (infrared-active) coupling vibrations of the molecules in the unit cell. Thus, for OsO_4 the correlation field splitting leads to nine Raman-active modes and nine infrared-active vibrations.

TABLE I

CORRELATION DIAGRAM FOR OsO_4

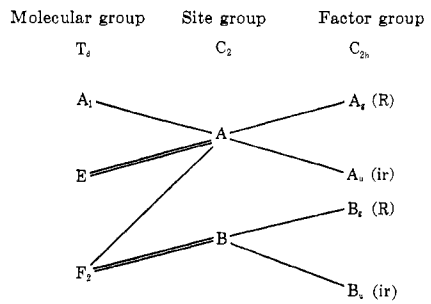

(1) G. Davidson, N. Logan, and A. Morris, *Chem. Commun.*, 1044 (1968).
(2) W. P. Griffiths, *J. Chem. Soc., A*, 1663 (1968).
(3) Details of the cell will be published at a later date.
(4) T. Ueki, A. Zalkin, and D. H. Templeton, *Acta Cryst.*, **19**, 157 (1965).

Figures 1 and 2 display the Raman spectrum of solid OsO_4 with the nine predicted components clearly

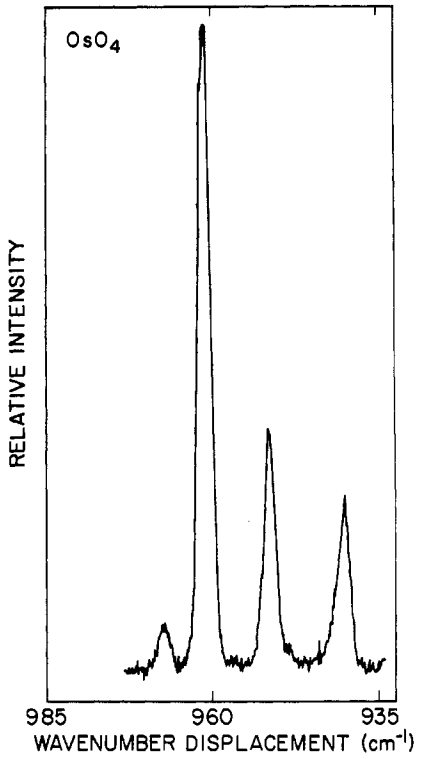

Figure 1.—The 950-cm^{-1} region of OsO_4. Instrumental conditions: slits, double 5 cm × ~1 cm^{-1}; sensitivity, 1.4 × 100; period, 2 sec; scan 0.05 cm^{-1} sec^{-1}; zero suppression, none.

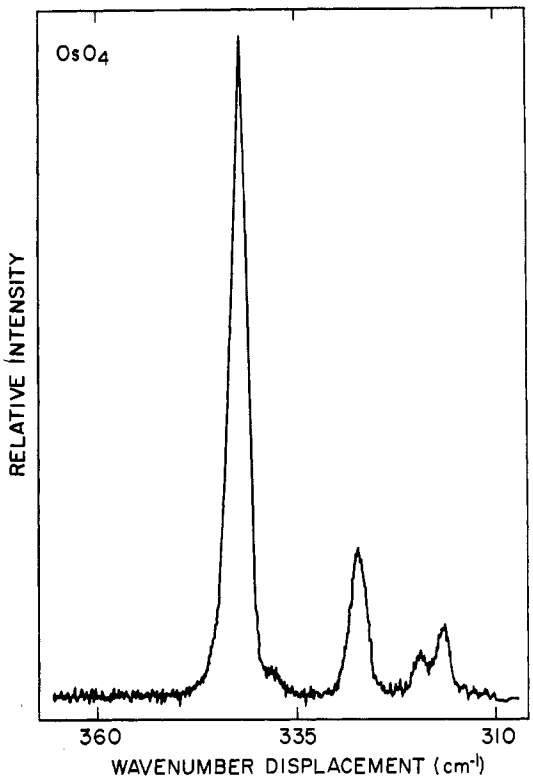

Figure 2.—The 330-cm^{-1} region of OsO_4. For instrumental conditions, see the caption to Figure 1.

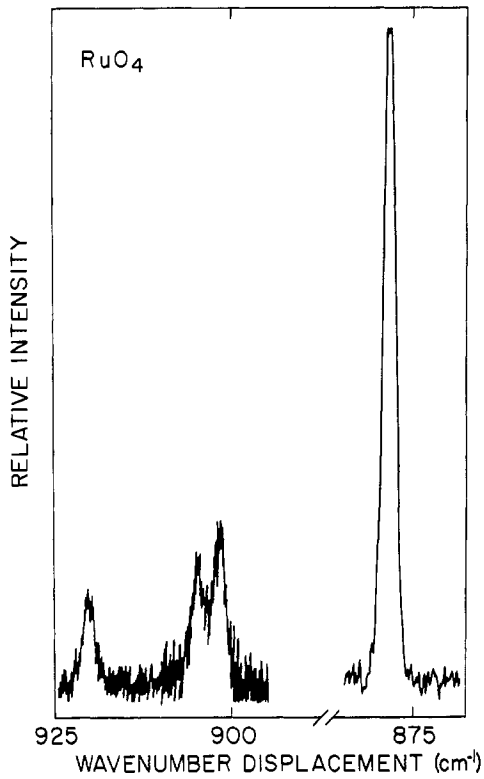

Figure 3.—The 900-cm^{-1} region of RuO_4. Instrumental conditions: slits, double 2.5 cm × ~1 cm^{-1}; sensitivity, 3000; period, 10 sec; scan 0.05 cm^{-1} sec^{-1}; zero suppression, none.

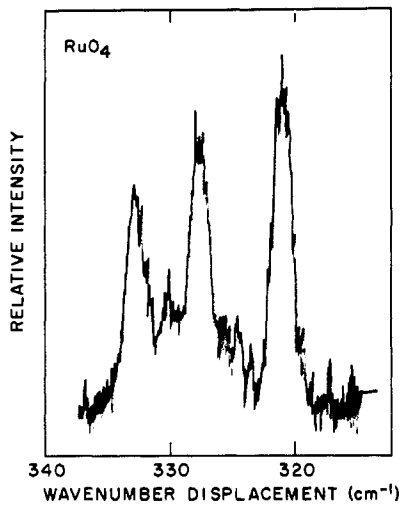

Figure 4.—The 330-cm^{-1} region of RuO_4. For instrumental conditions, see the caption to Figure 3.

resolved. Spectra of solid RuO_4, Figures 3 and 4, show analogous sets of multiplets, which suggest a similar crystal structure as that for OsO_4. Table II summarizes the vibrational data for both molecules. Since the E vibration of OsO_4 is split into a strong and a weak line, and not into two lines of nearly equal intensity, the possibility exists that the 338-cm^{-1} emission corresponds to the $Os^{16}O_3{}^{18}O$ species. The product rule suggests a shift of 5 cm^{-1} for the $Os^{16}O_3{}^{18}O$ vibration that is derived from the ν_2 mode of $Os^{16}O_4$. $Os^{16}O_3{}^{18}O$ occurs, however, in natural abundance at approximately 0.8%, which argues against the notion that the 338-cm^{-1} line belongs to this species. Figure 2 is a representative trace for this region; higher conditions of instrumental resolution failed to reveal any splitting in the more intense feature at 342 cm^{-1}. Since the structure at 338 cm^{-1} appeared in several samples of OsO_4, we rule out the possibility of an impurity and conclude that the line is a member of the split E vibration.

TABLE II

VIBRATIONAL FREQUENCIES FOR OsO_4 AND RuO_4

Assignment	Gas (infrared), cm^{-1}	Liquid (Raman), cm^{-1}	Crystal (Raman), cm^{-1}
	OsO_4		
ν_1 (A_1)		964[b]	961
ν_2 (E)		338[b]	342
			338
ν_3 (F_2)	959.5[a]	953[b]	967.5
			951.5
			940.0
ν_4 (F_2)	329.0[a]	334[b]	327
			319 [d]
			316
	RuO_4		
ν_1 (A_1)		883[c]	878
ν_2 (E)		338[c]	333
			330.5
ν_3 (F_2)	919.7[c]	918[c]	921
			905
			903
ν_4 (F_2)	329[c]	332[c]	328
			325.5
			321.5

[a] I. W. Levin and S. Abramowitz, *Inorg. Chem.*, **5**, 2024 (1966). [b] Reference 2. [c] I. W. Levin and S. Abramowitz, *J. Chem. Phys.*, in press. [d] Solid infrared frequencies are reported at 320 and 330 cm^{-1}: R. S. McDowell, *Inorg. Chem.*, **6**, 1759 (1967).

Unambiguous assignments for ν_2 and ν_4 for RuO_4 are difficult since the liquid Raman emission lines for these vibrations occur close to one another.[1,2] We tend to favor the higher value for ν_2 on the basis of the similar splitting patterns for OsO_4 and RuO_4 in the 330-cm^{-1} region of the two solids.

Although the spectra displayed in the figures were obtained from annealed films, it is interesting to compare these RuO_4 frequencies with the values from a sample in an amorphous (unannealed) phase. For the amorphous solid, only three frequencies are found in the 330-cm^{-1} region, namely, 331.5, 326, and 322.5 cm^{-1}. ν_1 remained at 878 cm^{-1}, but the frequencies associated with ν_3 appeared at 921, 912, and 904 cm^{-1}. Not only were the frequencies shifted in the amorphous phase, but the intensities were altered. For example, the relative intensities of the emission lines in the 330-cm^{-1} region of RuO_4 which are reproduced in ref 2 are analogous to the intensity ratios (about 5:8:3) that we found in the amorphous solid prior to annealing.

Since the difference in frequencies of the individual components in both the infrared and Raman spectra are a measure of the coupling between the molecules in the unit cell, we are attempting to locate for these solids the infrared-active crystal modes.

CONTRIBUTION FROM THE CHEMISTRY DEPARTMENT,
POLYTECHNIC INSTITUTE OF BROOKLYN,
BROOKLYN, NEW YORK 11201

The Electronic Structure of Manganese(V) in $Ca_2(PO_4)Cl$

BY J. MILSTEIN AND S. L. HOLT

Received November 4, 1968

Pursuant with our interest in the electronic structure of higher oxidation states[1-4] we wish to report on the single-crystal polarized spectrum of Mn(V) in the host $Ca_2(PO_4)Cl$. Single crystals of $Ca_2(PO_4)Cl$ containing small amounts of manganese were first prepared by Kingsley, *et al.*[5] Using various physical and chemical techniques they demonstrated that the manganese was present in the 5+ oxidation state and that it undoubtedly substituted for the phosphorous atom in the phosphate tetrahedron. In this study they also measured the absorption and emission spectrum of this compound but did not report polarization behavior as neither the structure of the host not that of the dopant was known at that time. Recently Greenblatt, *et al.*,[6] have determined the structures of both Ca_2PO_4Cl and Ca_2CrO_4Cl. On the basis of their data, the similarity of the polarization behavior between $Ca_2(PO_4,CrO_4)Cl$ and $Ca_2(PO_4,MnO_4)Cl$, and the electron spin resonance data of Banks,[7] *et al.*, for $Ca_2(PO_4,CrO_4)Cl$, we wish to suggest that the polarized spectrum of $Ca_2(PO_4,MnO_4)Cl$ is interpretable in terms of D_{2d} symmetry.

The spectrum of $Ca_2(PO_4,MnO_4)Cl$ at 80°K with light incident on the 001 crystal face is shown in Figure 1. No attempt was made to obtain the spectrum at lower temperatures as there is little physical difference between our 80°K spectrum and that reported for 2°K.[5]

The 80°K polarized spectrum of $Ca_2(PO_4,MnO_4)Cl$ was obtained using experimental techniques identical with those reported in earlier communications.[8,9]

Results and Discussion

Crystal field theory predicts that the energy level sequence for a d^2 ion in a tetrahedral environment should be $^3A_2 < {}^3T_2 < {}^3T_1(F) < {}^3T_1(P)$. The correlation between these states and those produced when tetrahedral symmetry is reduced to D_{2d} symmetry is shown in Table I.

TABLE I

T_d	D_{2d}
$^3A_2$	$^3B_1$
$^3T_2$	$^3B_2 + {}^3E$
$^3T_1$	$^3A_2 + {}^3E$

In the group D_{2d} the z component of the electric dipole transition operator is a function of symmetry B_2 while the x and y components of the operator belong to the E representation. The selection rules for allowed electric dipole transitions in D_{2d} symmetry are readily calculated. These are presented in Table II.

TABLE II

Initial and final states[a]	Transition symmetry	Allowed polarization directions
$^3B_1 \rightarrow {}^3E$	E	x, y
$^3B_1 \rightarrow {}^3B_2$	A_2	Forbidden
$^3B_1 \rightarrow {}^3A_2$	B_2	z

[a] Initial electron spin resonance measurements are, assuming D_{2d} symmetry, consistent with a $^3B_1$ ground state: J. Milstein, B. R. McGarvey, and S. L. Holt, unpublished data.

In Figure 1 we note that there are three areas of relatively intense absorption, 10,000–15,000, 15,000–20,000, and above 25,000 cm^{-1}. These absorptions have previously been assigned[5] as

$$^3A_2(t_1^6e^2) \rightarrow {}^3T_2(t_1^6et_2) \quad 11{,}000\ cm^{-1}$$
$$\rightarrow {}^3T_1(t_1^5e^3) \quad 13{,}800\ cm^{-1}$$
$$\rightarrow {}^3T_1(t_1^6et_2) \quad 17{,}500\ cm^{-1}$$
$$\rightarrow {}^3T_1(t_1^5e^2t_2) \quad 32{,}400\ cm^{-1}$$

Based upon this assignment but taking the molecular symmetry to be D_{2d} instead of T_d, we would expect that with $\vec{E} \perp z$ our spectrum should consist of absorptions in the regions of 11,000, 13,800, 17,500, and 32,400 cm^{-1}, *i.e.*, transitions from the $^3B_1$ ground state to the x,y-allowed low-symmetry components of the $^3T_2$ and $^3T_1$ states. On the other hand, with $\vec{E} \parallel z$ we should not see an 11,000-cm^{-1} band but should see the $^3A_2$ components at ~13,800, 17,500, and 32,400 cm^{-1}. Looking at Figure 1 we note that this behavior is not what is observed. While it is difficult to draw any conclusions about the weak 11,000-cm^{-1} absorption, clearly the band at 17,500 cm^{-1} does not have $^3T_1$ parentage as no component appears with $\vec{E} \parallel z$. The question is then, what kind of assignment can be made to explain the spectrum. One possible assignment is to treat all of the absorptions in the 9000–35,000-cm^{-1} region as arising from transitions occurring within the d manifold. Such an assignment would require that the first charge-transfer band in MnO_4^{3-} occur somewhere above 35,000 cm^{-1}. When one considers that the first charge-transfer transition occurs at ~18,000 cm^{-1} in both MnO_4^- and CrO_4^{3-} and at somewhat lower energies in MnO_4^{2-} it is

(1) S. L. Holt and C. J. Ballhausen, *Theoret. Chim. Acta*, **7**, 313 (1967).
(2) E. Banks, M. Greenblatt, and S. Holt, *J. Chem. Phys.*, **49**, 1431 (1968).
(3) J. Milstein and S. L. Holt, Abstracts, 156th National Meeting of the American Chemical Society, Atlantic City, N. J., Sept 1968, No. INOR 102.
(4) C. A. Kosky and S. L. Holt, ref 3, No. INOR 103.
(5) J. D. Kingsley, J. S. Prener, and B. Segall, *Phys. Rev.*, **137A**, 189 (1965).
(6) M. Greenblatt, E. Banks, and B. Post, *Acta Cryst.*, **23**, 166 (1967).
(7) E. Banks, M. Greenblatt, and B. R. McGarvey, *J. Chem. Phys.*, **47**, 3772 (1967).
(8) C. Simo and S. Holt, *Inorg. Chem.*, **7**, 2655 (1968).
(9) C. Simo, E. Banks, and S. L. Holt, *ibid.*, in press.